IEEE Open Journal of Vehicular Technology

Received 25 April 2023; accepted 23 May 2023. Date of publication 31 May 2023;
date of current version 15 June 2023. The review of this article was coordinated by Editor Chenhao Qi.

Digital Object Identifier 10.1109/OJVT.2023.3281723

A Digital Self-Interference Cancellation Scheme for In-Band Full-Duplex-Applied 5G System and Its Software-Defined Radio Implementation

SHOTA MORI [1,2] (Student Member, IEEE), KEIICHI MIZUTANI [1] (Member, IEEE), AND HIROSHI HARADA [1] (Member, IEEE)

[1]Graduate School of Informatics, Kyoto University, Kyoto 606-8501, Japan
[2] School of Platforms, Kyoto University, Kyoto 606-8501, Japan

CORRESPONDING AUTHOR: HIROSHI HARADA (email: hiroshi.harada@i.kyoto-u.ac.jp).

This work was supported by the Ministry of Internal Affairs and Communications in Japan under Grant JPJ000254. An earlier version of this paper was presented in part to the 2022 Annual IEEE International Symposium on Personal, Indoor and Mobile Radio Communications (IEEE PIMRC2022), Virtual Conference, Sep. 2022 [DOI: 10.1109/PIMRC54779.2022.9978126].

ABSTRACT The development of mobile communication technology toward 6G is difficult because the required spectrum resources have already been allocated to existing systems. Therefore, new communication systems must have high spectral efficiency to effectively utilize the available resources. This article proposes a digital self-interference (SI) canceller that can be applied to full-duplex cellular systems based on the current 5G signal format (5G-FDC) to introduce in-band full-duplex systems beyond 5G. Specifically, we reorganize the 5G demodulation reference signal (DMRS) and define a novel DMRS configuration, in which the DMRSs for uplink and downlink communications do not interfere with each other. The proposed DMRS configuration effectively improves the accuracy of the SI channel estimation. Moreover, we propose a channel extrapolation scheme that suppresses the channel estimation degradation, which deteriorates the block error rate performance. Additionally, we propose a noise estimation method to improve the low-density parity check decoding performance of the desired signal in 5G-FDC systems. The effectiveness of the proposed method is demonstrated through computer simulations and experimentally by using our developed and implemented software-defined radio-based 5G-FDC prototype. Digital SI cancellation performances of 50 dB and 30.6 dB are observed in the simulation and experimental evaluations, respectively.

INDEX TERMS 5G, full-duplex cellular, in-band full-duplex, self-interference, software-defined radio.

I. INTRODUCTION

The fifth-generation mobile communication system (5G) was launched in 2020 to satisfy various demands. It is standardized in three usage scenarios, which are selected based on the application performance requirements, as follows: massive machine-type communications (mMTC), ultra-reliable and low-latency communications (URLLC), and enhanced mobile broadband (eMBB) [2]. For 5G, a low-frequency band of 410–7125 MHz (frequency range 1: FR1) and a millimeter wave band of 24250–52600 MHz (FR2) ensure that the bandwidth satisfies the demands of various applications [2]. Furthermore, new technologies such as new radio (NR) and massive multiple-input multiple-output (MIMO) have been developed to achieve flexible and efficient usage of time and frequency resources [3]. However, applications such as cyber-physical systems [4], mission-critical Internet of things (IoT) [5], and vehicular-to-everything (V2X) [6], whose social implementation has increased significantly, require wireless communications that can accommodate an even larger number of terminals, and present a larger communication capacity and extremely low latency. Therefore, to satisfy these demands, the development of mobile communication technology must

move toward sixth-generation mobile communication system (6G), particularly in terms of capacity and latency performance [7]. This process requires the utilization of additional spectrum resources. However, these resources have already been allocated to existing radio systems and cannot be allocated for any further development in mobile communications, especially in FR1 (i.e., Sub-6 GHz) [8].

The in-band full-duplex (IBFD) technology presents considerable potential to improve spectral efficiency [9], [12], [13], [14], [15], [16], [17], [18], [19], [20], [21], [22], [23], [24], [25], [26], [27], [28], [29], [30], [31]. In this approach, transmission and reception are performed simultaneously using the same frequency resources, which can ideally achieve twice the spectral efficiency of conventional half-duplex (HD) systems [9], [10], [11], [12]. Several studies have been conducted on the application of IBFD in wireless fidelity (Wi-Fi) and other applications [13], [14], [15]. Some recent studies have also applied IBFD for cellular (i.e., full-duplex cellular (FDC)) systems to advance the development of mobile communications beyond 5G [16], [17], [18], [19], [20], [21], [22], [23], [24], [25], [26], [27], [28]. Most existing FDC systems are based on user-paired IBFD (UP-IBFD), in which the base station (BS) simultaneously receives uplink (UL) signals from one user equipment (UE) and transmits downlink (DL) signals to another UE. In this study, we refer to the UL signal transmitting UE as UL-UE, and to the DL signal receiving UE as DL-UE. There are three additional interferences in UP-IBFD-based FDC systems when compared to the HD-based conventional cellular systems: self-interference (SI) at the BS, inter-UE interference (IUI), and inter-cell interference (ICI). A dynamic duplex cellular (DDC) system was developed to avoid or mitigate IUI and ICI through the selection and scheduling of the UL-UEs and DL-UEs to be paired in the UP-IBFD and by using a transmit power control algorithm [16], [17]. Furthermore, while the IUI can be spatially attenuated by the distance between the UL-UE and DL-UE, a method to successively cancel the IUI through digital signal processing has also been proposed [18]. One of the major problems in an FDC system is the implementation of SI cancellation at the BS.

Generally, there are two types of SI cancellation schemes: passive suppression and active cancellation. The passive suppression schemes reduce the power level of the SI by using antenna directionality and arrangement, a radio frequency (RF) absorber, and cross-polarization to attenuate the line-of-sight (LoS) component [19], [20], [21]. The active cancellation schemes generate a copy of the SI signal and subtract it from the received signal [1], [13], [22], [23], [24], [25], [26], [27], [28]. Active cancellation can be implemented in both analog and digital domains (i.e., analog SI cancellation and digital SI cancellation). In practice, passive suppression, analog SI cancellation, and digital SI cancellation must be combined to suppress the SI to the desired power level. For example, [13] proposed a 110 dB cancellation scheme, wherein a 60 dB cancellation was achieved using passive suppression and analog SI cancellation, and a Wi-Fi system was used to achieve the 50 dB digital SI cancellation. The analog SI cancellation schemes suppress the SI component using an analog circuit before inputting the received signal into an analog-to-digital converter (ADC) [13], [22], [23], [24]. It is essential to prevent the saturation of the input level and the deterioration of the desired signal due to quantization noise [11]. Conversely, the digital SI cancellation schemes can completely remove the residual SI component through digital signal processing [1], [13], [25], [26], [27], [28]. In this approach, the replica signal is generated using the SI channel, which is estimated using the reference signals contained within the SI signal. The generated replica signal is then subtracted from the received signal in the digital domain. For example, recently, a digital SI cancellation scheme based on the signal configuration of long-term evolution (LTE) has been proposed [26]. However, to the best of our knowledge, there have been no studies conducted on digital SI cancellation for the application of IBFD technology to 5G systems, considering the 5G signal configuration and the impact on the performance of low-density parity-check (LDPC) code. Additionally, almost all of the previous studies on SI cancellation schemes (e.g., [20], [22], [23], [24], [27], [28]) focus only on SI power reduction and do not evaluate the performance of UL communications during IBFD operation. In [13], it was demonstrated that IBFD improves the throughput in full-duplex Wi-Fi links using actual equipment. However, detailed UL communication performance, such as BLER performance as a function of signal-to-interference-plus-noise power ratio (SINR), which is required for adaptive modulation to operate cellular systems, has not been shown.

In this study, we propose a digital SI canceller that can be applied to an FDC system based on the current 5G signal format (5G-FDC) to introduce IBFD systems beyond 5G. Furthermore, we propose a noise estimation method to improve the LDPC decoding performance of the desired signal in a 5G-FDC system. A major problem in digital SI cancellers is the deterioration of the accuracy of SI channel estimation by the desired signal [1], [26], [29]. In 5G, the demodulation reference signal (DMRS) is used for channel estimation and equalization; the 5G-FDC also requires this DMRS to estimate the SI channel and generate an SI replica signal. However, using the 5G DMRS produces interference between the DMRS of the DL signal (i.e., the SI signal) and the DMRS of the UL signal (i.e., the desired signal). This deteriorates the accuracy of the SI channel estimation and SI replica signal generation. Consequently, the digital SI cancellation accuracy deteriorates, and the communication quality of the desired signal also deteriorates. In this study, we rearrange the 5G DMRS and define a novel DMRS configuration in which the DMRS for the UL communication (UL-DMRS) and the DMRS for the DL communication (DL-DMRS) do not interfere with each other. The proposed DMRS configuration improves the accuracy of the SI channel estimation.

In our earlier and shorter version of this study [1], we proposed the aforementioned 5G-FDC and digital SI canceller using the defined UL-DMRS and DL-DMRS. We also proposed a method for noise estimation using the proposed DMRS structure; this is required to decode the LDPC codes, which are applied as error-correcting codes in 5G. The proposed schemes are evaluated through computer simulations. In this study, we extend the above studies by developing a 5G-FDC physical (PHY) layer prototype that implements the proposed method using a software-defined radio (SDR) platform to demonstrate the feasibility of the proposed scheme. Since the actual transmitted signal is based on time division duplex (TDD), there exist channel extrapolation portions in the forward and backward slots, which degrade the channel estimation accuracy. Therefore, we propose a channel extrapolation scheme to suppress the degradation of the channel estimation accuracy in the channel extrapolation part; this degradation may otherwise lead to performance deterioration in the block error rate (BLER), which is an implementation problem. The effectiveness of the proposed scheme is demonstrated through computer simulations and an experimental evaluation, which is performed using the developed SDR-based 5G-FDC prototypes and measurement equipment. The purpose of this study is to improve the spectral efficiency in the Sub-6 GHz band using IBFD. Therefore, coexistence with massive-multiple-input multiple-output (MIMO) [30], [31] used in the millimeter wave band is not assumed.

The main contributions of this study can be summarized as follows:

- A novel DMRS configuration for the 5G-FDC is proposed; a digital SI canceller with SI channel estimation is developed using the proposed DMRS configuration to introduce IBFD beyond 5G [1].
- A channel extrapolation scheme is proposed to improve the channel estimation accuracy.
- A scheme for estimating the noise, which is required for LDPC decoding, is proposed to improve the communication quality of the desired UL signal when applying the 5G-FDC [1].
- A performance evaluation of the PHY layer of the 5G-FDC, including the proposed schemes, is performed through computer simulation.
- A prototype of the PHY layer 5G-FDC including the proposed schemes is developed using SDRs, and the performance of the 5G-FDC PHY layer is experimentally evaluated.

The remainder of this article is organized as follows. Section II presents an overview of the 5G PHY layer. Section III presents the proposed digital SI cancellation approach, including the DMRS configuration, channel extrapolation scheme, and noise estimation scheme. Section IV presents the performance evaluation of the proposed 5G-FDC PHY layer performance through computer simulation. Section V presents the developed SDR-based 5G-FDC PHY prototype and experimental evaluation results. Finally, Section VI concludes the article.

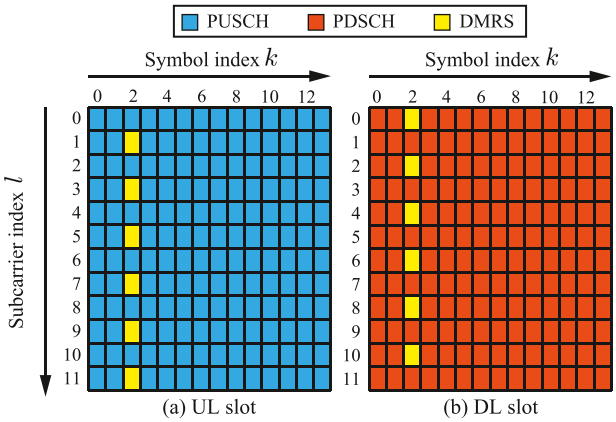

FIGURE. 1. Conventional resource allocation example in a 5G system.

II. 5G PHYSICAL LAYER

This section presents an overview of the 5G PHY layer, particularly the DMRS configuration and LDPC decoding, which must be considered for the SI cancellation in the 5G-FDC system.

A. DMRS CONFIGURATION

The orthogonal frequency-division multiplexing (OFDM) scheme is adopted as the transmission scheme in 5G, and the PHY resource-allocation unit is defined as a resource block (RB) comprising one OFDM symbol in the time domain and 12 subcarriers in the frequency domain [32]. A unit comprising one OFDM symbol and one subcarrier is called a resource element (RE). Essentially, each RE is assigned a role, such as a PHY UL/DL shared channel (PUSCH/PDSCH) for information transmission and DMRS for channel estimation. Fig. 1 presents an example of resource allocation in a slot (i.e., consecutive 14 OFDM symbols). The DMRS layout method varies based on the channel characteristics in the frequency and time domains. A maximum of four DMRSs can be placed in the time domain [32]. In this study, we assumed that one DMRS is placed in a slot.

B. LDPC DECODING

5G adopts a binary LDPC code, which is a linear block code that uses a sparse parity check matrix for the error correction code of PUSCH/PDSCH [33]. The log-domain sum-product algorithm, which is an iterative method, is generally used to decode the LDPC code owing to its simple implementation. The accuracy of the log-likelihood ratio (LLR) calculation significantly affects the error correction performance since the LLR is input to the LDPC decoder.

Assuming the HD system, the i-th received signal, y_i, is expressed as

$$y_i = h_i x_i + n_i, \tag{1}$$

where h_i, x_i, and n_i represent the i-th complex channel gain, transmitted symbol, and additive white Gaussian noise

(AWGN) with a power of σ^2, respectively. Here, the definition of the LLR of the j-th bit in the i-th symbol, $\lambda_i(j)$, is expressed as follows:

$$\lambda_i(j) = \log \frac{P(y_i|x_i(j)=0)}{P(y_i|x_i(j)=1)}. \tag{2}$$

In the AWGN environment (i.e., $h_i = 1$), $\lambda_i(j)$ is calculated as follows:

$$\lambda_i(j) = \log \frac{\sum_{u\in U_0^j} e^{-\frac{1}{\sigma^2}\left(\left(x-u_x^j\right)^2+\left(y-u_y^j\right)^2\right)}}{\sum_{u\in U_1^j} e^{-\frac{1}{\sigma^2}\left(\left(x-u_x^j\right)^2+\left(y-u_y^j\right)^2\right)}}, \tag{3}$$

where x and y represent the in-phase and quadrature coordinates of the received signal points, respectively. U_0^j and U_1^j represent the ideal constellation points whose j-th bits are 0 and 1, respectively. The in-phase and quadrature coordinates of U_0^j and U_1^j are denoted as u_x^j and u_y^j, respectively.

The number of elements in U_0^j and U_1^j increases with the increase in the modulation level, and the computational complexity increases exponentially. To reduce the processing time of the LLR calculation, the approximate LLR was calculated as follows [34]:

$$\lambda_i(j) = -\frac{1}{\sigma^2}\left(\min_{u\in U_0^j}\left(\left(x-u_x^j\right)^2+\left(y-u_y^j\right)^2\right) - \min_{u\in U_1^j}\left(\left(x-u_x^j\right)^2+\left(y-u_y^j\right)^2\right)\right). \tag{4}$$

Here, only the nearest ideal constellation points among U_0^j and U_1^j from the received signal point are used to calculate the denominator and numerator of (3). In this study, we used (4) to decode the 64QAM signal.

Even in a fading environment, the LLR can be calculated as shown in (4) by multiplying (1) by the inverse of the estimated channel, $\tilde{h}_i^{-1}(\approx h_i^{-1})$, and compensating the noise term as follows:

$$\sigma'^2 = \left|\tilde{h}_i\right|^{-2}\sigma^2. \tag{5}$$

The absolute value of LLR is inversely proportional to σ^2, as shown in (3) and (4). Therefore, it becomes extremely high in a high signal-to-noise power ratio (SNR) environment. Consequently, the error correction of the LDPC does not work since the plus/minus sign of LLR, which determines the bit after decoding, cannot be changed during the limited iterations of the sum-product algorithm only when the sign is miscalculated. The LLR clipping method [34] is implemented in this study to overcome this problem. The clipped LLR is expressed as follows:

$$\lambda_i'(j) = \begin{cases} \lambda_i(j) & (|\lambda_i(j)| \le \varphi) \\ \mathrm{sgn}(\lambda_i(j))\cdot\varphi & (|\lambda_i(j)| > \varphi) \end{cases}, \tag{6}$$

where, $\mathrm{sgn}(\cdot)$ represents a sign function and φ (> 0) denotes the upper limit of the absolute value of the LLR. In this study, φ is set to 10.

III. PROPOSED DIGITAL SI CANCELLER FOR THE 5G-FDC

This section explains the proposed digital SI cancellation, including the DMRS configuration, channel extrapolation scheme, and noise estimation scheme for the 5G-FDC.

A. PROPOSED SI CANCELLATION SYSTEM MODEL

Fig. 2 presents a block diagram of the BS with the proposed SI cancellation method. The hardware imperfections in the power amplifiers (PAs), low-noise amplifiers (LNAs), analog-to-digital converters (ADCs), and digital-to-analog converters (DACs) were considered in this study. The proposed digital SI cancellation scheme aims to remove the residual SI component by assuming that some passive suppression and analog SI cancellation operate linearly. When operating the IBFD, the received signal of the BS in the digital domain Y, is expressed as follows:

$$Y = H^{\mathrm{SI}}X^{\mathrm{DL}} + H^{\mathrm{UL}}X^{\mathrm{UL}} + N, \tag{7}$$

where X^{DL} and X^{UL} represent the UL and DL signals, respectively; H^{SI} and H^{UL} represent the SI and UL channels, respectively; and N denotes AWGN. Here, uppercase letters represent frequency-domain representations. Since X^{DL} is always known to the BS, the SI signal component can be cancelled by generating the replica signal of the SI signal component, $\tilde{H}^{\mathrm{SI}}X^{\mathrm{DL}}$, where $\tilde{H}^{\mathrm{SI}}$ represents the estimated value of H^{SI}, and subtracting it from the received signal as follows:

$$\begin{aligned} Y' &= Y - \tilde{H}^{\mathrm{SI}}X^{\mathrm{DL}} \\ &= \left(H^{\mathrm{SI}} - \tilde{H}^{\mathrm{SI}}\right)X^{\mathrm{DL}} + H^{\mathrm{UL}}X^{\mathrm{UL}} + N \end{aligned} \tag{8}$$

where Y' denotes the signal after processing the digital SI cancellation. (8) shows that the estimation accuracy of the SI channel leads to the residual SI component, $(H^{\mathrm{SI}} - \tilde{H}^{\mathrm{SI}})X^{\mathrm{DL}}$, having a significant effect on the demodulation accuracy of the desired signal. Therefore, it is crucial to improve the estimation accuracy of H^{SI}.

Furthermore, the residual SI component may affect the LLR calculation. Assuming that the residual SI signal follows a Gaussian distribution, the LLR used for decoding is calculated as follows when QPSK is applied:

$$\lambda_i(j) = \log \frac{\sum_{u\in U_0^j} e^{-\frac{1}{\sigma^2+\sigma_{\mathrm{SI}}^2}\left(\left(x-u_x^j\right)^2+\left(y-u_y^j\right)^2\right)}}{\sum_{u\in U_1^j} e^{-\frac{1}{\sigma^2+\sigma_{\mathrm{SI}}^2}\left(\left(x-u_x^j\right)^2+\left(y-u_y^j\right)^2\right)}}, \tag{9}$$

where σ_{SI}^2 represents the power of the residual SI component after digital SI cancellation. Additionally, the approximate LLR used for decoding when 64QAM is applied is calculated

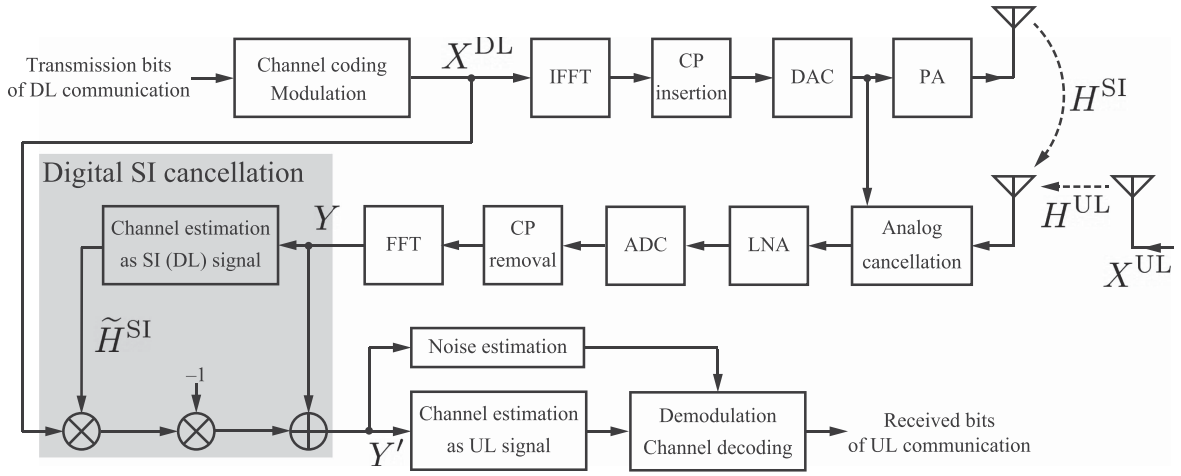

FIGURE. 2. Block diagram of BS with the proposed SI cancellation.

as follows:

$$\lambda_i(j) = -\frac{1}{\sigma^2+\sigma_{\mathrm{SI}}^2}\left(\min_{u\in U_0^j}\left(\left(x-u_x^j\right)^2+\left(y-u_y^j\right)^2\right)\right.$$
$$\left.-\min_{u\in U_1^j}\left(\left(x-u_x^j\right)^2+\left(y-u_y^j\right)^2\right)\right) \tag{10}$$

B. PROPOSED DMRS CONFIGURATION

A high estimation accuracy of the SI channel must be achieved by using the DMRS, which is already defined for 5G. However, during the operation of the IBFD, the estimation accuracy of the SI channel may deteriorate since the UL and DL signals interfere with each other. Therefore, the UL-DMRS and DL-DMRS configurations must be designed cooperatively. Since it is assumed that the current 5G system cannot be used in the operation of the IBFD, we developed a novel DMRS configuration for the IBFD, which can avoid interference between the DL-DMRS and PUSCH and between the UL-DMRS and PDSCH.

Fig. 3 illustrates the proposed DL-DMRS and UL-DMRS configurations. Here, the DL-DMRS and UL-DMRS were placed in separate REs to avoid interference. Furthermore, in the UL slot, null subcarriers were allocated instead of PUSCH in the second symbol to prevent PUSCH from interfering with the DL-DMRS. Similarly, in the DL slot, null subcarriers were allocated instead of PDSCH in the second symbol to prevent PDSCH from interfering with the UL-DMRS. The proposed configurations enable the BS to receive DL-DMRS and UL-DMRS without contamination from the other signals. Consequently, H^{SI}, which is required for SI cancellation along with H^{UL}required for the demodulation of the UL signal (i.e., the desired signal) can be estimated with high accuracy. The proposed configuration reduces the number of REs in the UL and/or DL slot. However, the total throughput of the system is expected to be approximately doubled since the UL and DL communications can be operated simultaneously. Therefore, the proposed DMRS configuration effectively improves the spectral efficiency.

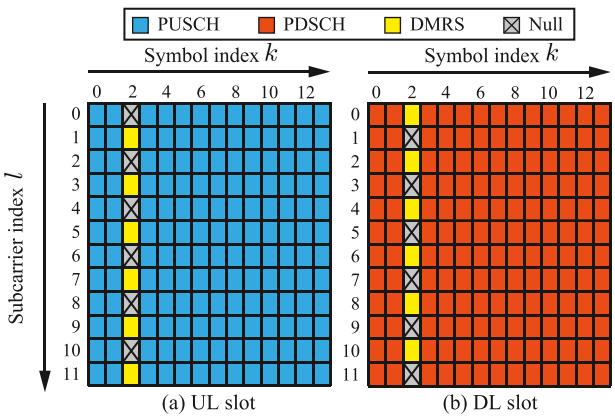

FIGURE. 3. Proposed resource allocation for the 5G-FDC.

C. PROPOSED NOISE POWER ESTIMATION SCHEME

In 5G, the receiver must have an estimating function of the noise power σ^2 for LDPC decoding, as shown in (3) and (4). Previous studies have proposed several noise power estimation schemes. For instance, [35] proposed a method based on the correlation of a cyclic prefix (CP) which does not require a known signal. Since the IBFD operation is assumed in this study, a noise estimation scheme that is unaffected by the residual SI signals is required. Therefore, we propose a noise estimation scheme in the frequency domain based on [36] and [37] using a known UL-DMRS, which is unaffected by the residual SI signal. This scheme can be operated without new overhead in both the HD and IBFD operations.

The received UL-DMRS, which is allocated to the l-th subcarrier of k-th symbol $Y_{k,l}^{\mathrm{ULD}}$, is expressed as follows:

$$Y_{k,l}^{\mathrm{ULD}} = H_{k,l}^{\mathrm{ULD}} X_{k,l}^{\mathrm{ULD}} + N_{k,l}^{\mathrm{ULD}}, \tag{11}$$

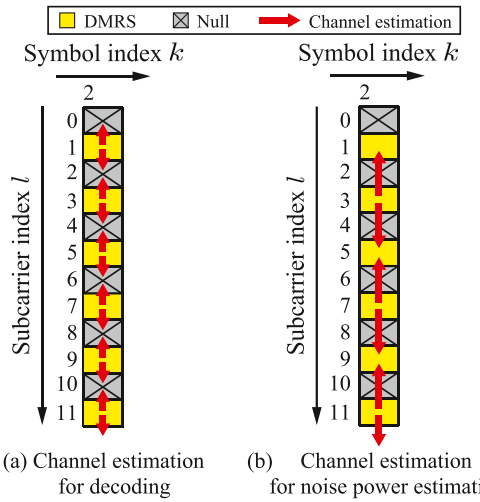

FIGURE. 4. Difference of channel estimation according to the usages.

where $H_{k,l}^{\mathrm{ULD}}$, $X_{k,l}^{\mathrm{ULD}}$, and $N_{k,l}^{\mathrm{ULD}}$ represent the channel gain, transmitted UL-DMRS, and noise components of the l-th subcarrier of the k-th symbol, respectively. Here, the RE located on the k $(= 0, 1, \ldots, K-1)$-th in the time domain and l $(= 0, 1, \ldots, L-1)$-th in the frequency domain are expressed as (k, l), respectively, where K and L represent the number of REs in the time and frequency domains, respectively. Similar to [36] and [37], the noise power can be estimated as follows:

$$\widetilde{\sigma^2} = \mathrm{E}\left[\left|Y_{k,l}^{\mathrm{ULD}} - \tilde{H}_{k,l}^{\mathrm{ULD}} X_{k,l}^{\mathrm{ULD}}\right|^2\right], \tag{12}$$

where $\widetilde{\sigma^2}$ and $\tilde{H}_{k,l}^{\mathrm{ULD}}$ represent the estimated values of the noise power, and $H_{k,l}^{\mathrm{ULD}}$, respectively, and $\mathrm{E}[\cdot]$ denotes the expected value.

According to (12), $\tilde{H}_{k,l}^{\mathrm{ULD}}$ must be obtained. Typically, the channel of all the UL-DMRS, $\tilde{H}_{2,2m+1}^{\mathrm{ULD}}(m = 0, 1, \ldots, L/2-1)$, is estimated during the demodulation process of the desired signal, as shown in Fig. 4(a).

However, the calculation result of (12) becomes $\widetilde{\sigma^2} = 0$ because $\tilde{H}_{2,2m+1}^{\mathrm{ULD}}$ is calculated as $\tilde{H}_{2,2m+1}^{\mathrm{ULD}} = Y_{2,2m+1}^{\mathrm{ULD}} / X_{2,2m+1}^{\mathrm{ULD}}$ to estimate the RE channel at $(2, 2m)$ using linear interpolation or extrapolation. Therefore, we propose the channel estimation method of the UL-DMRS, which uses half of the UL-DMRS to estimate the channel of the other half alternately, as shown in Fig. 4(b). $\tilde{H}_{2,4n+3}^{\mathrm{ULD}}$ $(n = 0, 1, \ldots, L/4-1)$ is calculated as $\tilde{H}_{2,4n+3}^{\mathrm{ULD}} = Y_{2,4n+3}^{\mathrm{ULD}} / X_{2,4n+3}^{\mathrm{ULD}}$, and is used to estimate $\tilde{H}_{2,4n+1}^{\mathrm{ULD}}$ through linear interpolation or extrapolation. The noise power is then estimated according to (12) with $\tilde{H}_{2,4n+1}^{\mathrm{ULD}}$.

D. PROPOSED CHANNEL EXTRAPOLATION METHOD

When transmitting and receiving consecutive n (≥ 2) slots using the DMRS configuration shown in Fig. 3, the extrapolation parts for the channel estimation exist in the head and tail slots, as shown in Fig. 5. In particular, in the tail slot (e.g., slot 4 in Fig. 5), the ratio of channel estimation through extrapolation is considerably large. This extrapolation deteriorates the accuracy of the channel estimation of the SI and UL channels and the LLR calculation, which deteriorates BLER. Therefore, we propose a channel extrapolation method to suppress the performance deterioration caused by extrapolation by using the averaging process of multiple slots. This work assumes an environment where there are no objects around the BS and the UE moves at a low speed, the channel variation in the time domain can be considered as approximately linear, and the accuracy of channel extrapolation is degraded primarily by the noise.

Assuming that consecutive n slots are received and the channel estimation value of RE located on (k, l) is expressed as $\tilde{H}_{k,l}$, the channel estimation value of the OFDM symbol containing DMRS, $\tilde{H}_{k_i^{\mathrm{D}},l}$, is first obtained, as shown in Fig. 4(a). Here, k_i^{D} denotes the i $(= 1, \ldots, K^{\mathrm{D}})$-th symbol index containing the DMRS, and K^{D} denotes the number of symbols containing the DMRS in consecutive n slots. Subsequently, channel interpolation is performed by calculating the channel-time variation for each subcarrier. Lastly, when extrapolating in the head and tail slots, the average channel time variation for each subcarrier, V_l^{ave}, is calculated as follows:

$$V_l^{\mathrm{ave}} = \frac{1}{K^{\mathrm{D}}-1} \sum_{i=1}^{K^{\mathrm{D}}-1} \frac{\tilde{H}_{k_{i+1}^{\mathrm{D}},l} - \tilde{H}_{k_i^{\mathrm{D}},l}}{14}. \tag{13}$$

The channel is then extrapolated using V_l^{ave} from the channel-estimated values $\tilde{H}_{k_1^{\mathrm{D}},l}$ and $\tilde{H}_{k_{K^{\mathrm{D}}}^{\mathrm{D}},l}$ as start points.

IV. PERFORMANCE EVALUATION BY COMPUTER SIMULATIONS

In this section, we evaluate the performance of the proposed digital SI cancellation method in a computer simulation. We considered the UL signal as the desired signal and the DL signal as the SI signal.

A. EVALUATION BY COMPUTER SIMULATION

Table I lists the simulation parameters for the computer simulation. The antennas of the UL and DL are assumed to be single-input single-output (SISO) antennas. The DMRS configurations of the UL and DL signals were set to the same ones shown in Fig. 3. Both the UL and DL signals use 64QAM modulation. The channel model of the UL signal was set to the TDL-A model defined by 3GPP [38], which can change the delay spread arbitrarily based on the simulation environment. In this study, we set the delay spread to 100 ns, which is the median value of the non-line-of-sight (NLoS) environment. Conversely, the SI channel was set to one-tap Rician fading, which contains a line-of-sight (LoS) component from the transmitting antenna to the receiving antenna of the BS, and NLoS components reflected by the objects around the BS. The power ratio of the LoS component to the NLoS component is called the Rician factor, α. In this computer simulation, we set $\alpha = 20$ dB. Additionally, the maximum Doppler frequencies

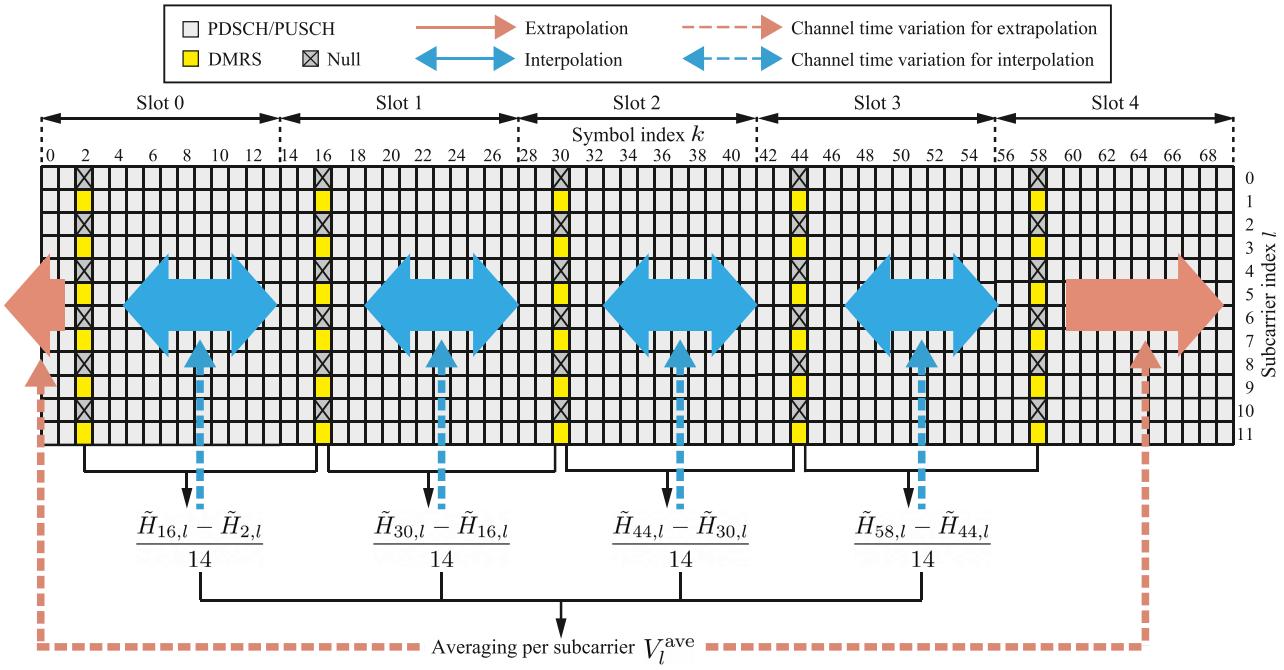

FIGURE. 5. **Proposed channel extrapolation for 5G-FDC.**

TABLE 1. **Evaluation Parameters**

Parameter	Value
Channel bandwidth	20 MHz
Subcarrier spacing	15 kHz
Allocated bandwidth	106 PRBs
FFT size	2,048
CP rate	144/2,048 (all symbols)
Coding scheme	LDPC
Modulation Scheme,	MCS7 (QPSK), $R = 526/1{,}024$
Code Rate R	MCS19 (64QAM), $R = 517/1{,}024$
Transport block size	MCS7: 2,112 bytes
	MCS19: 6,273 bytes
Decoding algorithm	Log-domain sum-product
Decoding iteration	50
Carrier frequency	4.0 GHz
UL Channel	TDL-A [38], Delay spread: 100 ns
SI Channel	Rician fading
Moving speed	3 km/h (11.1 Hz)
Antenna	Tx: 1, Rx, 1

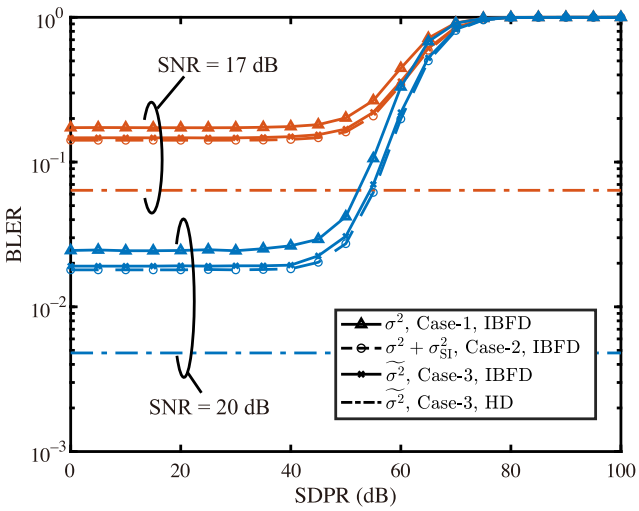

FIGURE. 6. **BLER characteristics as a function of SDPR depending on the noise term in the LLR calculation.**

of the UL and SI channels were set to 11.1 Hz, which assumes that the UL-UE and the objects around the UL-UE and BS move at 3 km/h. The effectiveness of the proposed SI cancellation method was evaluated based on the BLER performance of the desired UL signal. In this evaluation, three consecutive superimposed UL and DL slots were transmitted, but only their center slots were demodulated for BLER evaluation and they remained unaffected by the channel extrapolation.

Fig. 6 depicts the BLER characteristics of the UL signal when IBFD is applied as a function of the SI signal power-to-desired signal power ratio (SDPR), which indicates the power ratio of the residual SI signal component after passive suppression and analog SI cancellation of the desired signal component. When the SNR was 17 dB and 20 dB, the BLER characteristics in the three cases relating to the noise terms in the LLR calculation were evaluated as follows:

Case-1: The ideal noise power, σ^2, is used for the LLR calculation according to (4).

Case-2: σ^2 and the residual SI power after the proposed digital SI cancellation, σ_{SI}^2, were used for the LLR calculation according to (10).

Case-3: The estimated noise power, $\widetilde{\sigma^2}$, calculated from (12), was used for the LLR calculation according to (4).

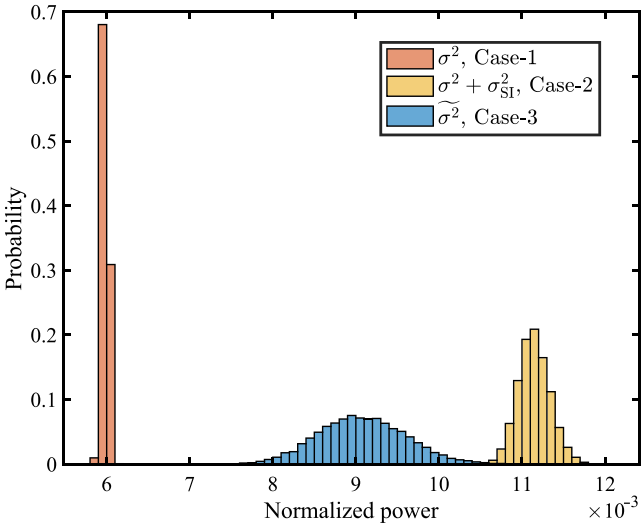

FIGURE. 7. Distributions of noise, and residual SI power, and estimated noise power used for the LLR calculation.

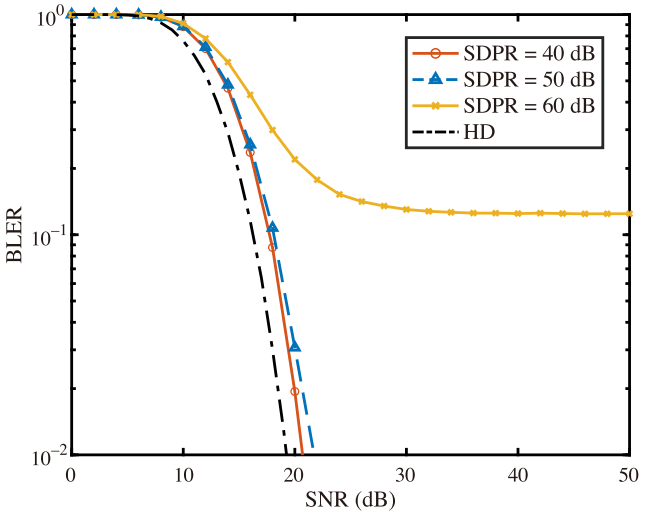

FIGURE. 8. BLER characteristics as a function of SNR.

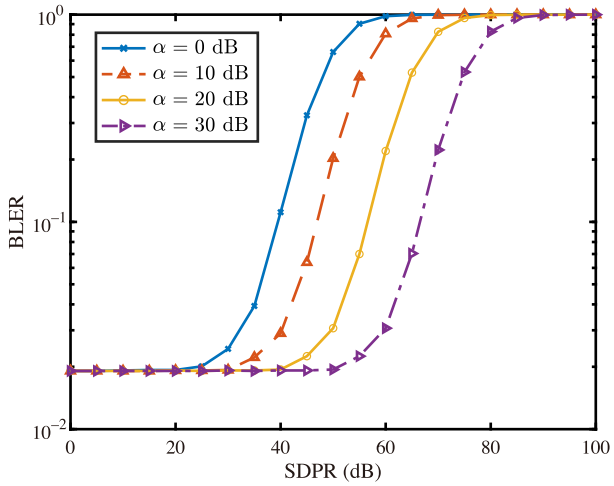

FIGURE. 9. BLER characteristics as a function of SDPR depending on Rician factor.

For comparison, the BLER characteristics during the HD operation are depicted in Fig. 6. In the SDPR range of 0–40 dB, the BLER is a constant value regardless of the LLR calculation method. This indicates that the proposed SI cancellation scheme can sufficiently suppress the SI signals. However, the BLER in the IBFD operation is worse than that in the HD operation, primarily because the residual SI power makes the effective SINR smaller than the SNR due to the estimation error of the SI channel. In the SDPR range above 40 dB, the BLER deteriorates with the increase in the SDPR due to the high power of the SI signal, such that the residual SI power significantly reduces the effective SINR.

Subsequently, when considering the LLR calculation methods, the order of the best BLER characteristics was Case-2, Case-3, and Case-1. Thus, if the noise and residual SI power are known, the LLR must be calculated according to (10). Consequently, these powers must be estimated. Here, the BLER characteristics of Case-3, which were obtained using the estimated noise power, were better than those of Case-1, which were obtained using the ideal noise power. It is assumed that the channel estimation error for the noise estimation scheme increases the $\widetilde{\sigma^2}$ value closer to $\sigma^2 + \sigma_{\mathrm{SI}}^2$, rather than σ^2. To support this hypothesis, Fig. 7 presents the distributions of σ^2, $\sigma^2 + \sigma_{\mathrm{SI}}^2$, and $\widetilde{\sigma^2}$ for SDPR = 40 dB and SNR = 20 dB. The horizontal axis represents the noise power normalized by the desired signal power. Fig. 7 clearly demonstrates that the BLER characteristics of Case-3 are better than those of Case-1 since the distribution of $\widetilde{\sigma^2}$ is closer to $\sigma^2 + \sigma_{\mathrm{SI}}^2$ than that of σ^2. Hereafter, LLR is only calculated according to Case-3 for practical cases.

Fig. 8 depicts the BLER characteristics of the UL signal when IBFD is applied as a function of SNR under SDPR conditions of 40 dB, 50 dB, and 60 dB. The effect of HD is also illustrated. Even when the SDPR is set to 40 dB and 50 dB, the proposed SI cancellation enables the BLER to decrease with an increase in the SNR, as shown in Fig. 8. However, the BLER characteristics deteriorate by 1–2 dB when compared to those of HD. This is because the effective SINR decreases due to the residual SI power, as mentioned above. Conversely, when the SDPR is 60 dB, the BLER converges to 0.12 due to the performance limitation of the proposed SI cancellation scheme. Therefore, if the passive suppression and analog SI cancellation schemes can reduce the SDPR to 50 dB or lower, the proposed SI cancellation scheme can maintain the communication quality of the IBFD almost identical to that of the HD.

Fig. 9 depicts the BLER characteristics as a function of the SDPR under the conditions of SNR = 20 dB and α = 0, 10, 20, and 30 dB. The larger the Rician factor, the greater the permissible amount of SDPR that does not deteriorate the BLER. When α was set to 0, 10, 20, and 30 dB, the

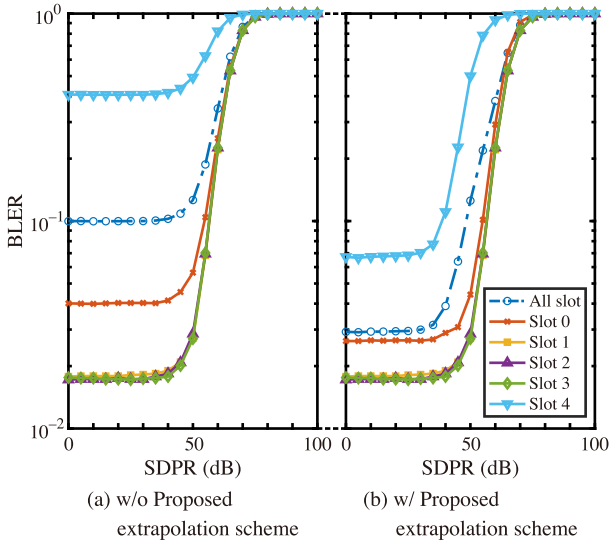

FIGURE. 10. BLER characteristics as a function of SDPR depending on channel extrapolation scheme.

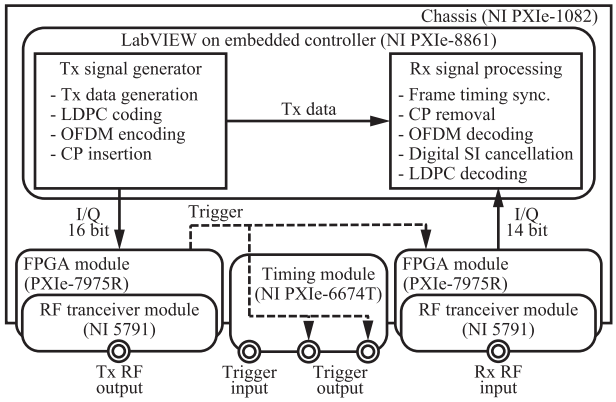

FIGURE. 11. Configuration of the BS.

TABLE 2. Equipment List

Equipment	Product model
SDR devices	
・Chassis	PXIe-1082, NI
・Embedded controller	PXIe-8861, NI
・RF adapter module	NI-5791, NI
・FPGA module	PXIe-7975R, NI
・Synchronization module	PXIe-6674T, NI
Baseband signal processor	LabVIEW, NI
	MATLAB 2021b, MathWorks
Variable attenuator (VATT)	8494A, Keysight
	8494B, Keysight
	8496A, Keysight
	8496B, Keysight
Signal combiner	PD510-0S, R&K
	PD610-0S, R&K

permissible amounts of SDPR were 20, 30, 40, and 50 dB, respectively. Thus, the performance of the proposed SI cancellation scheme changes due to the Rician factor, which varies based on the passive suppression and analog SI cancellation scheme implemented on the BS, and a cooperative design of SI cancellation schemes is essential to realize the IBFD in an actual system.

Lastly, we evaluate the proposed extrapolation scheme. In this evaluation, five consecutive superimposed UL and DL slots were transmitted, and all the UL slots were demodulated to evaluate the BLER, as shown in Fig. 5. Fig. 10 depicts the BLER characteristics for each slot and the average BLER characteristics of all the slots as a function of the SDPR under the conditions of $\alpha = 20$ dB and SNR $= 20$ dB. Figs. 10(a) and (b) depicts the evaluation results with and without the proposed extrapolation scheme, respectively. In the SDPR range of 0–40 dB, the BLER is a constant value, regardless of the extrapolation scheme. However, its values vary based on the slot, and the order of the best BLER characteristics is the 1st–3rd, 0th, and 4th slots. In particular, when the proposed extrapolation scheme is not used, the BLER of the 4th slot is 0.41, which is considerably worse than that of the other slots, as shown in Fig. 10(a). Conversely, the proposed extrapolation scheme improves the BLER of the 4th slot to 0.07, as shown in Fig. 10(b). The BLER of the 0th slot was also improved. The average BLER improved from 0.10 to 0.03, which verifies the effectiveness of the proposed extrapolation method.

V. DEVELOPMENT OF 5G-FDC PHYSICAL LAYER PROTOTYPE AND FUNDAMENTAL EVALUATION

A. CONFIGURATION OF BS

Fig. 11 depicts the BS configuration and Table II lists the specifications of the equipment used in the study. Two radio frequency (RF) modules (5791, National Instruments (NI)) connected to two field programmable gate arrays (FPGA) modules (PXIe-7975R, NI), an embedded controller (PXIe-8861, NI), and a synchronization module (PXIe-6674T, NI) were installed in a chassis (PXIe-1082, NI) with a high-speed local bus. The RF modules correspond to a frequency range of 200 MHz to 4.4 GHz and a bandwidth of up to 100 MHz.

Firstly, the signal processing software (LabVIEW and MATLAB) in the embedded controller generates a 5G digital baseband signal. Subsequently, the in-phase and quadrature (I/Q) digital signal is written into the RF module for transmission (Tx-RFm) and converted into an analog signal by using a 16-bit DAC. The analog signal is upconverted to an RF signal and transmitted based on the trigger signal generated by the Tx-RFm. This trigger signal is supplied to the RF module for reception (Rx-RFm) via the high-speed local bus of the chassis. Rx-RFm starts receiving when the trigger signal is detected. Therefore, the BS simultaneously transmits and receives the RF signal.

Rx-RFm converts the received RF signal into a baseband signal and then converts it into an I/Q digital signal using a 14-bit ADC. The 14-bit digital signal is converted to a 16-bit digital signal on the FPGA and transmitted to the embedded

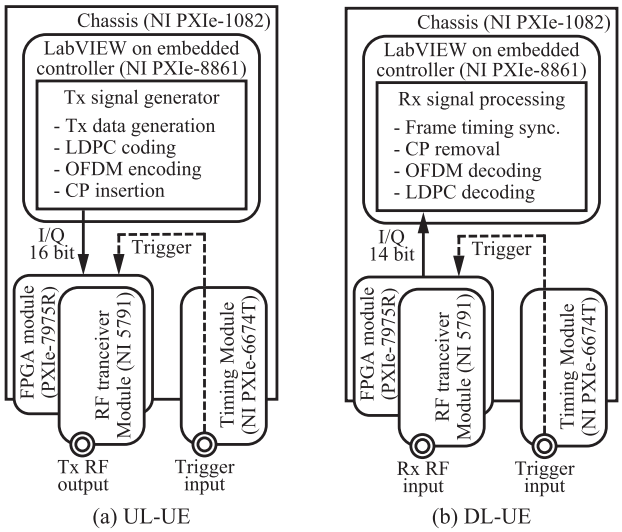

FIGURE. 12. Configurations of the UEs.

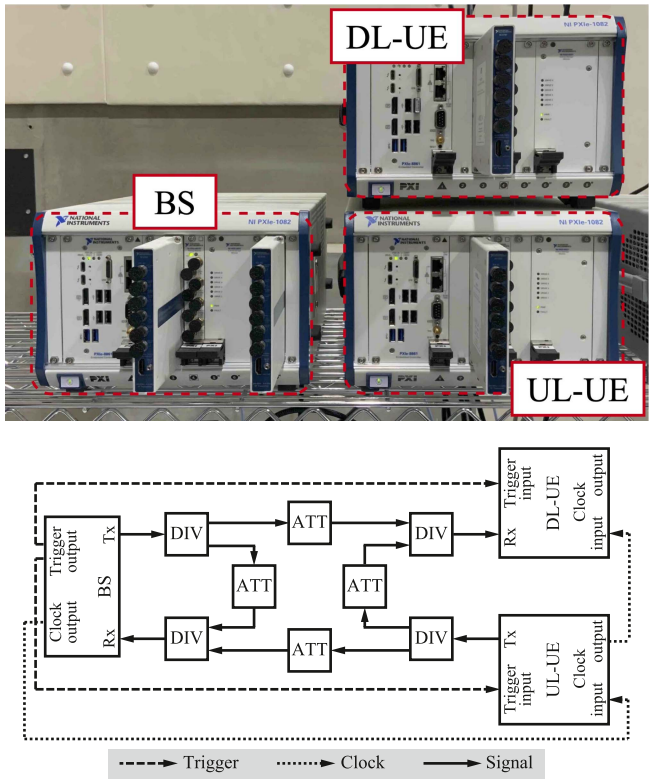

FIGURE. 13. Connection structure of the proposed 5G-FDC PHY prototype.

controller via the high-speed local bus of the chassis. Reception processing, including the digital SI cancellation process explained in Section III, is then performed. Subsequently, Tx-RFm generates the trigger signal again, and the next procedures for transmitting and receiving signals are started. Therefore, the 5G-FDC PHY prototype is a semi-real-time system which transmits and receives the signal intermittently. Additionally, the trigger signal is output through the synchronization module to synchronize the transmitting and receiving timing of the UL-UE and DL-UE with the BS.

B. CONFIGURATION OF UE

Fig. 12(a) and (b) present the configurations of the UL-UE and DL-UE, respectively. Essentially, the configurations of UE are identical to that of the BS. However, only one RF module is equipped, which is used for transmission or reception, namely, Tx-RFm or Rx-RFm. When the trigger signal transmitted from BS is detected via the synchronization module, the Tx-RFm on UL-UE and Rx-RFm on DL-UE start transmitting and receiving, respectively. Similar to the BS, the embedded controllers generate and demodulate the 5G baseband signal using the signal processing software.

C. CONNECTION STRUCTURE OF 5G-FDC PHY PROTYPE

Fig. 13 depicts the connection structure of the proposed 5G-FDC PHY prototype. The DL signal transmitted by the BS is input to the receivers of the DL-UE and BS via the signal combiners. Similarly, the UL signal transmitted by the UL-UE is inputted to the receiver of the DL-UE and BS. Attenuators (ATT) were inserted into these four paths. Therefore, the received power of the UL and DL signals and the strength of the SI and IUI can be flexibly varied by adjusting the attenuation amount. The effectiveness of various technologies to realize the IBFD in different environments can be verified by inserting a fading emulator into the path. Additionally, an external analog SI cancellation can be inserted in the SI path. In this study, the 10 MHz reference clock signal output from the rear surface of the chassis of the BS is input to the UL-UE and DL-UE in series (i.e., daisy chain) for sharing.

D. EVALUATION BY 5G-FDC PHY PROTOTYPE

In this evaluation, we used the proposed 5G-FDC PHY prototype. The simulation parameters are almost identical to those listed in Table I, except for the carrier frequency, modulation scheme, code rate, and propagation channel. The carrier frequency was set to 2.15 GHz. For the fundamental evaluation, we used QPSK modulation and set the UL and SI channels to AWGN (i.e., not inserting a fading emulator). The output power of the Tx-RFm of the BS and UL-UE was fixed at –15 dBm, and the SDPR and SNR were varied by adjusting the ATTs of the UL and SI channels. In particular, varying the ATT of the SI channel corresponded to linear passive suppression and analog SI cancellation. In this evaluation, five consecutive superimposed UL and DL slots were transmitted, and all the UL slots were demodulated for BLER evaluation, as shown in Fig. 5. The timing synchronization is based on the autocorrelation of the CP.

Subsequently, we evaluated the performance of the proposed digital SI cancellation based on the power spectrum density (PSD). In this evaluation, the ATTs of the UL and SI channels were set to 110 dB and 10 dB, respectively, to focus on the SI signal. Fig. 14 depicts the PSDs of the received

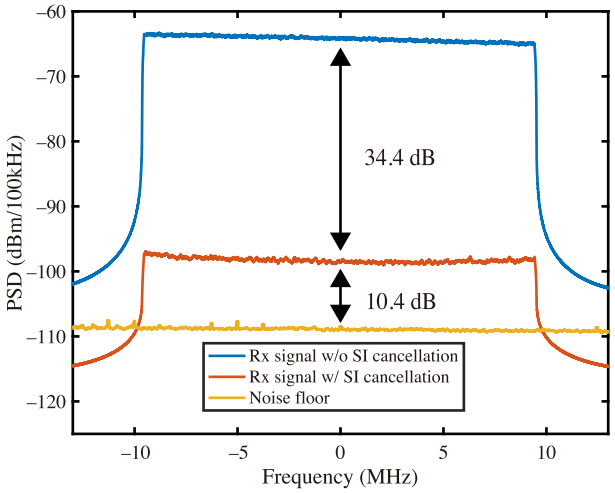

FIGURE. 14. Measured power spectrum densities.

signals with and without the proposed SI cancellation. For comparison, the observed noise floor was illustrated by setting the ATT of the SI channel to 110 dB. The proposed digital SI cancellation scheme achieved a cancellation of approximately 34.4 dB, as shown in Fig. 14. This result is considered to be appropriate since it is almost identical to the linear SI cancellation scheme in [25]. However, the PSD after the proposed digital SI cancellation is 10.4 dB larger than that of the noise floor because the nonlinear component of the SI signal is not sufficiently removed. Therefore, it is essential to develop and introduce nonlinear digital SI cancellation to further improve the cancellation performance.

Fig. 15(a) and (b) depict the BLER characteristics of the UL communication for each slot and the averaged BLER characteristics of all the slots with and without the proposed extrapolation scheme, respectively, as a function of the SDPR. The ATT of the UL channel was fixed at 40 dB and that of the SI channel was set to be variable in this evaluation. When operating the HD, the received power of the UL signal and noise power are measured at -76.5 and -89.9 dBm, respectively. The SNR of the desired signal is approximately 13.4 dB, which is the environment in which the BLER is less than 10^{-3}.

The order of the best BLER characteristics is 2nd, 1st, 3rd, 0th, and 4th slots as shown in Fig. 15(a) and (b). However, the BLER characteristics of the 4th slot, i.e., the tail slot, are very poor because of the extrapolation effect, particularly in Fig. 15(a). Therefore, the averaged BLER is less than 0.1 in the range of SDPR $\leq$ 27.7 dB. Conversely, the averaged BLER is less than 0.1 in the range of SDPR $\leq$ 30.6 dB since the proposed extrapolation scheme improves the BLER characteristics of the 4th and 0th slots. Therefore, the effectiveness of the proposed digital SI cancellation and channel extrapolation scheme is demonstrated using actual equipment. The SI cancellation performance is low when compared to the computer simulation since hardware imperfections such as the nonlinearity of the PA and quantization noise are not

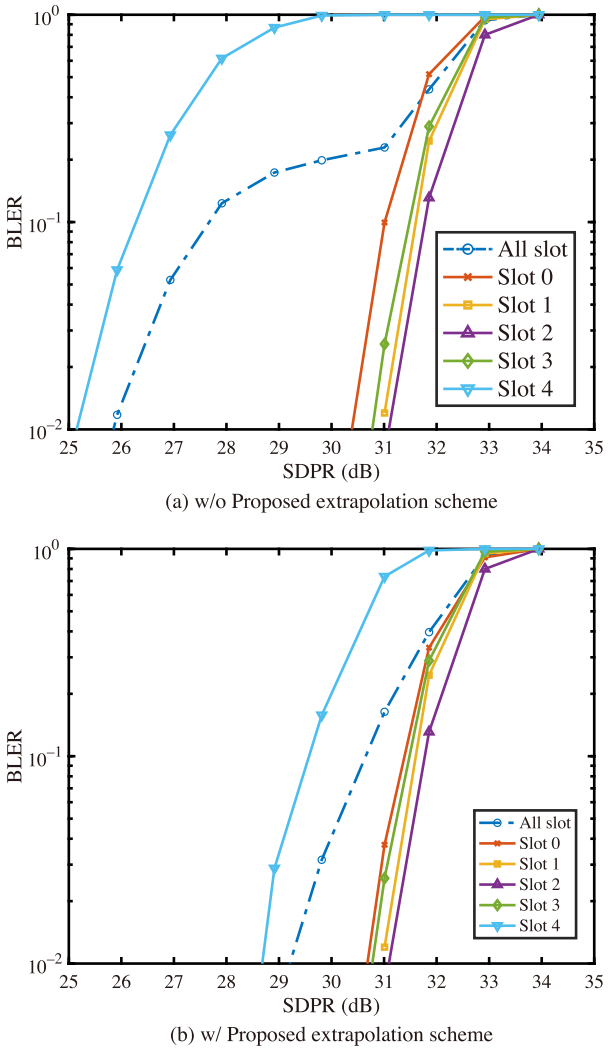

FIGURE. 15. BLER characteristics as a function of SDPR obtained by the proposed 5G-FDC PHY prototype.

considered in the computer simulation, and the proposed SI cancellation only suppresses the linear components of the SI signal. To realize 5G-FDC in an actual system in the future, these problems must be solved and the SI cancellation performance must be improved.

VI. CONCLUSION

This study proposes a digital SI canceller that can be applied to FDC systems based on the current 5G signal format to introduce IBFD beyond 5G. To this end, we reorganized the 5G DMRS and defined a novel DMRS configuration in which the UL-DMRS and DL-DMRS did not interfere with each other. Moreover, we proposed a channel extrapolation scheme that suppresses the channel estimation degradation at the channel extrapolation part, which deteriorates the performance of the BLER. Additionally, we proposed a noise estimation method to improve the LDPC decoding performance of the desired signal in 5G-FDC systems. The effectiveness of the proposed method is demonstrated through both computer simulations as

well as experimental evaluation using an SDR-based 5G-FDC prototype that we developed and implemented. We verified the effectiveness of the proposed digital SI cancellation scheme, which achieved a cancellation performance of 50 dB and 30.6 dB in the simulation and experiment, respectively. These results demonstrate the possibility of realizing FDC in 5G systems. In the future, we aim to design a nonlinear digital SI cancellation scheme for 5G signals to improve the SI cancellation performance and validate it using the proposed prototype.

REFERENCES

[1] S. Mori, K. Mizutani, and H. Harada, "Digital self-interference cancellation for full-duplex cellular system in 5G," in *Proc. IEEE 33rd Annu. Int. Symp. Pers., Indoor Mobile Radio Commun.*, 2022, pp. 1165–1170.

[2] A. Ghosh, A. Maeder, M. Baker, and D. Chandramouli, "5G evolution: A view on 5G cellular technology beyond 3GPP Release 15," *IEEE Access*, vol. 7, pp. 127639–127651, 2019.

[3] 3GPP, "Base Station (BS) radio transmission and reception," 3GPP Tech. Specification 38.104 V16.4.0, Jul. 2020.

[4] K. M. Alam and A. El Saddik, "C2PS: A digital twin architecture reference model for the cloud-based cyber-physical systems," *IEEE Access*, vol. 5, pp. 2050–2062, 2017.

[5] F. Ciccozzi, I. Crnkovic, D. Di Ruscio, I. Malavolta, P. Pelliccione, and R. Spalazzese, "Model-driven engineering for mission-critical IoT systems," *IEEE Softw.*, vol. 34, no. 1, pp. 46–53, Jan./Feb. 2017.

[6] M. H. C. Garcia et al., "A tutorial on 5G NR V2X communications," *IEEE Commun. Surv. Tut.*, vol. 23, no. 3, pp. 1972–2026, thirdquarter 2021.

[7] M. Z. Chowdhury, M. Shahjalal, S. Ahmed, and Y. M. Jang, "6G wireless communication systems: Applications, requirements, technologies, challenges, and research directions," *IEEE Open J. Commun. Soc.*, vol. 1, pp. 957–975, 2020.

[8] Ministry of Internal Affairs and Communications, Japan, *Current Situation of Spectrum Use in Japan*. Tokyo, Japan: Ministry Intern. Affairs Commun., 2022.

[9] A. Sabharwal, P. Schniter, D. Guo, D. W. Bliss, S. Rangarajan, and R. Wichman, "In-band full-duplex wireless: Challenges and opportunities," *IEEE J. Sel. Areas Commun.*, vol. 32, no. 9, pp. 1637–1652, Sep. 2014.

[10] S. Goyal, P. Liu, S. S. Panwar, R. A. Difazio, R. Yang, and E. Bala, "Full duplex cellular systems: Will doubling interference prevent doubling capacity?," *IEEE Commun. Mag.*, vol. 53, no. 5, pp. 121–127, May 2015.

[11] K. Mizutani and H. Harada, "Quantization noise reduction by digital signal processing-assisted analog-to-digital converter for in-band full-duplex systems," *IEEE Trans. Wireless Commun.*, vol. 21, no. 8, pp. 6643–6655, Aug. 2022.

[12] D. Kim, H. Lee, and D. Hong, "A survey of in-band full-duplex transmission: From the perspective of PHY and MAC layers," *IEEE Commun. Surv. Tut.*, vol. 17, no. 4, pp. 2017–2046, Fourthquarter 2015.

[13] D. Bharadia, E. McMilin, and S. Katti, "Full duplex radios," in *Proc. ACM SIGCOMM Comput. Commun. Rev.*, 2013, pp. 375–386.

[14] S. Shaboyan, A. S. Behbahani, and A. M. Eltawil, "Active cancellation of self-interference for full-duplex amplify and forward Wi-Fi relay," *IEEE Wireless Commun. Lett.*, vol. 7, no. 6, pp. 1050–1053, Dec. 2018.

[15] I. Ahn, J. Kim, and H. Song, "Adaptive analog self-interference cancellation for in-band full-duplex wireless communication," in *Proc. IEEE Asia-Pacific Microw. Conf.*, 2019, pp. 414–416.

[16] T. Matsumura, H. Kuriki, K. Mizutani, and H. Harada, "Macrocell capacity enhancement with dynamic full-duplex cellular system," in *Proc. 21st Int. Symp. Wireless Pers. Multimedia Commun.*, 2018, pp. 336–341.

[17] K. Nishikori, K. Teramae, K. Mizutani, T. Matsumura, and H. Harada, "User throughput enhancement with dynamic full-duplex cellular system in dense urban multi-cell environment," in *Proc. IEEE 30th Annu. Int. Symp. Pers., Indoor Mobile Radio Commun.*, 2019, pp. 1–6.

[18] S. Mori, K. Mizutani, and H. Harada, "In-band full-duplex-applicable area expansion by inter-user interference reduction using successive interference cancellation," *IEICE Trans. Commun.*, vol. E105-B, no. 2, pp. 168–176, Feb. 2022.

[19] E. Everett, A. Sahai, and A. Sabharwal, "Passive self-interference suppression for full-duplex infrastructure nodes," *IEEE Trans. Wireless Commun.*, vol. 13, no. 2, pp. 680–694, Feb. 2014.

[20] K. E. Kolodziej, J. P. Doane, B. T. Perry, and J. S. Herd, "Adaptive beamforming for multi-function in-band full-duplex applications," *IEEE Wireless Commun.*, vol. 28, no. 1, pp. 28–35, Feb. 2021.

[21] K. Fukushima, S. Mori, K. Mizutani, and H. Harada, "Single-cell dynamic duplex cellular system using distributed receive-only base stations," in *Proc. IEEE 95th Veh. Technol. Conf.*, 2022, pp. 1–5.

[22] T. Matsumura, "On the analog self-interference cancellation for in-band full-duplex radio with compensation for inherent frequency response," in *Proc. IEEE 24th Int. Symp. Wireless Pers. Multimedia Commun.*, 2021, pp. 1–6.

[23] A. Ershadi and K. Entesari, "A 0.5-to-3.5 GHz self-interference canceling receiver for in-band full-duplex wireless," in *Proc. IEEE Radio Freq. Integr. Circuits Symp.*, 2019, pp. 151–154.

[24] D. Korpi et al., "Full-duplex mobile device: Pushing the limits," *IEEE Commun. Mag.*, vol. 54, no. 9, pp. 80–87, Sep. 2016.

[25] M. S. Sim, M. Chung, D. Kim, J. Chung, D. K. Kim, and C.-B. Chae, "Nonlinear self-interference cancellation for full-duplex radios: From link-level and system-level performance perspectives," *IEEE Commun. Mag.*, vol. 55, no. 9, pp. 158–167, Sep. 2017.

[26] E. Ahmed and A. M. Eltawil, "All-digital self-interference cancellation technique for full-duplex systems," *IEEE Trans. Wireless Commun.*, vol. 14, no. 7, pp. 3519–3532, Jul. 2015.

[27] M. Erdem, O. Gurbuz, and H. Ozkan, "Integrated linear and nonlinear digital cancellation for full duplex communication," *IEEE Wireless Commun.*, vol. 28, no. 1, pp. 20–27, Feb. 2021.

[28] J. Tamminen et al., "Digitally-controlled RF self-interference canceller for full-duplex radios," in *Proc. 24th Eur. Signal Process. Conf.*, 2016, pp. 783–787.

[29] Y. Morikawa, K. Mizutani, and H. Harada, "Highly efficient demodulation scheme for in-band full-duplex using heterogeneous wireless communication schemes," in *Proc. IEEE 94th Veh. Technol. Conf.*, 2021, pp. 1–5.

[30] X. Xia, K. Xu, Y. Wang, and Y. Xu, "A 5G-enabling technology: Benefits, feasibility, and limitations of in-band full-duplex mMIMO," *IEEE Veh. Technol. Mag.*, vol. 13, no. 3, pp. 81–90, Sep. 2018.

[31] K. Xu, Z. Shen, Y. Wang, X. Xia, and D. Zhang, "Hybrid time-switching and power splitting SWIPT for full-duplex massive MIMO systems: A beam-domain approach," *IEEE Trans. Veh. Technol.*, vol. 67, no. 8, pp. 7257–7274, Aug. 2018.

[32] 3GPP, "Physical channels and modulation," 3GPP Tech. Specification 38.211 V15.2.0, Jun. 2018.

[33] 3GPP, "Multiplexing and channel coding," 3GPP Tech. Specification 38.212 V15.2.0, Jun. 2018.

[34] S. Schwandter, P. Fertl, C. Novak, and G. Matz, "Log-likelihood ratio clipping in MIMO-BICM systems: Information geometric analysis and impact on system capacity," in *Proc. IEEE Int. Conf. Acoust., Speech Signal Process.*, 2009, pp. 2433–2436.

[35] F. X. Socheleau, A. Aissa-El-Bey, and S. Houcke, "Non data-aided SNR estimation of OFDM signals," *IEEE Commun. Lett.*, vol. 12, no. 11, pp. 813–815, Nov. 2008.

[36] H. Arslan and S. Reddy, "Noise power and SNR estimation for OFDM based wireless communication systems," in *Proc. IASTED Int. Conf. Wireless Opt. Commun.*, 2003, pp. 1–6.

[37] D. J. Shin, W. Sung, and I. K. Kim, "Simple SNR estimation methods for QPSK modulated short bursts," in *Proc. IEEE Glob. Telecommun. Conf.*, 2001, pp. 3644–3647.

[38] 3GPP, "Study on channel model for frequencies from 0.5 to 100 GHz," 3GPP Tech. Rep. 38.901 V14.3.0, Jan. 2018.

SHOTA MORI (Student Member, IEEE) received the B.E. degree from the Faculty of Engineering, Kyoto University, Kyoto, Japan, in 2021, and the M.I. degree in 2023 from the Graduate School of Informatics, Kyoto University, where he is currently working toward the Ph.D. degree. His research interests include physical layer technologies of 6th generation mobile communication (6G) system. He was the recipient of the Student Paper Award from IEEE VTS Tokyo/Japan Chapter in 2021 and the Student Award from IEICE technical committee on SRW in 2022.

KEIICHI MIZUTANI (Member, IEEE) received the B.E. degree in engineering from the Osaka Prefecture University, Sakai, Japan, in 2007, and the M.E. and Ph.D. degrees in engineering from the Tokyo Institute of Technology, Tokyo, Japan, in 2009 and 2012, respectively. He is currently an Associate Professor with the Graduate School of Informatics, Kyoto University, Kyoto, Japan. He was an Invited Researcher with Fraunhofer Heinrich Hertz Institute, Berlin, Germany, in 2010. From April 2012 to September 2014, he was a Researcher with the National Institute of Information and Communications Technology (NICT), Tokyo. From October 2014 to December 2021, he was an Assistant Professor of the Graduate School of Informatics, Kyoto University. From January 2021 to September 2022, he was an Associate Professor with the School of Platforms, Kyoto University. He currently Researches the topics of physical layer technologies in white space communications, dynamic spectrum access, wireless smart utility networks (Wi-SUN), and 4G/5G/6G systems, including OFDM, OFDMA, MIMO, multihop relay network, and full-duplex cellular systems. Since joining NICT, he has been involved in IEEE 802 standardization activities, namely 802.11af, 802.15.4m, and 802.22b. He was the recipient of the Special Technical Awards from IEICE SR technical committee in 2009 and 2017, Best Paper Award from IEICE SR technical committee in 2010 and 2020, Young Researcher's Award from IEICE SRW technical committee in 2016, Best Paper Award from WPMC2017 and WPMC2020, and Best Paper Presentation Award (1st Place) from IEEE WF-IoT 2020.

HIROSHI HARADA (Member, IEEE) is currently a Professor with the Graduate School of Informatics, Kyoto University, Kyoto, Japan, and an Research Executive Director of the Wireless Networks Research Center, National Institute of Information and Communications Technology (NICT), Tokyo, Japan. In 1995, he joined the Communications Research Laboratory, Ministry of Posts and Communications, (currently, NICT). From 2005 to 2014, he was a Visiting Professor with the University of Electro-Communications, Tokyo. Since 1995, he has researched software defined radio, cognitive radio, dynamic spectrum access network, wireless smart ubiquitous network, and broadband wireless access systems on VHF, UHF, microwave, and millimeter-wave bands. In 2014, he was a Professor with Kyoto University. He has authored the book titled *Simulation and Software Radio for Mobile Communications* (Artech House, 2002). He has also joined many standardization committees and forums in the United States as well as in Japan and fulfilled important roles in them, especially IEEE 1900 and IEEE 802. He was the Chair of IEEE DySpan Standards Committee and Vice Chair of IEEE 802.15.4g, IEEE 802.15.4m, 1900.4, and TIA TR-51. He was the Board of Directors of IEEE communication society standards board, SDR forum, DSA alliance, and WhiteSpace alliance. He is the Co-founder of Wi-SUN alliance and was the Chairman of the board from 2012 to 2019. He is currently the Vice Chair of IEEE 2857, IEEE 802.15.4aa, and Wi-SUN alliance. He was the Chair of the IEICE Technical Committee on Software Radio (TCSR) and the Chair of Public Broadband Mobile Communication Development Committee, ARIB. He is also involved in many other activities related to telecommunications. He was the recipient of the achievement awards in 2006 and 2018 and Fellow of IEICE in 2009 and the achievement awards of ARIB in 2009, 2018, and 2022, respectively, on the topic of research and development of cognitive radio and wireless smart utility network.